Available online at www.sciencedirect.com

ScienceDirect

Ceramics International 42 (2016) 1545–1551

CERAMICS INTERNATIONAL

www.elsevier.com/locate/ceramint

Mechanochemical synthesis of MnZn ferrite nanoparticles suitable for biocompatible ferrofluids

Mercedes Arana[a], Paula G. Bercoff[a,*], Silvia E. Jacobo[b], Pedro Mendoza Zélis[c], Gustavo A. Pasquevich[c]

[a]*Facultad de Matemática, Astronomía y Física, Universidad Nacional de Córdoba, IFEG, Conicet, Córdoba, Argentina*
[b]*LAFMACEL, Universidad de Buenos Aires. INTECIN, Conicet, Buenos Aires, Argentina*
[c]*IFLP-Conicet. Departamento de Física, Facultad de Ciencias Exactas, Universidad Nacional de La Plata, Argentina*

Received 12 August 2015; accepted 18 September 2015
Available online 26 September 2015

Abstract

$Mn_{0.4}Zn_{0.6}Fe_2O_4$ nanoparticles (NPs) were synthesized by the mechanochemical method, starting from elemental oxides. Structural and magnetic properties of the NPs were investigated by X ray diffraction (XRD), vibrating sample magnetometry (VSM) and both scanning and transmission electron microscopy (SEM and TEM). XRD measurements show that MnZn ferrite is already present after 15 min of milling. After milling for 120 min, the resulting powder is almost completely single-phase without the need of any thermal treatment. Magnetization curves for samples with different milling times show saturation magnetizations ranging from 12.2 emu/g –after 15 min to 50.3 emu/g –after 120 min. Coercive field and remanent magnetization are negligible for all samples, in agreement with a superparamagnetic behavior. NPs with mean size of 8 nm were separated by centrifugation and were coated with chitosan for the preparation of a ferrofluid, which showed good stability for 12 h. The Intrinsic Loss Parameter (ILP) of this fluid indicates that the mechanochemical method can be a good alternative for the synthesis of the usual Fe-oxides ferrofluids used in hyperthermia.

Keywords: Mechanochemistry; MnZn nanoparticles; Biocompatible ferrofluid

1. Introduction

Mechanical milling in a high-energy ball mill is recognized as an effective way of producing solid-state chemical reactions at low temperatures. This mechanical process induces chemical reactions in powder precursors during the collisions with the grinding media, favoring the formation of fine (nanosized) particles [1,2]. The underlying mechanism of mechanochemical process is repeated deformation, fracture, and welding of the powder charge during collisions of the grinding media. Fracture of particles exposes fresh reacting surfaces and welding generates interfaces between reactant phases across which short-range diffusion can occur, thus allowing chemical reactions to take place without kinetic constraint. Diffusion rates are also enhanced by the high concentration of lattice defects, which provide shorter diffusion paths [3,4].

The mechanochemical synthesis process is appropriate to produce soft magnetic materials such as ferrites [5]. From a stoichiometric mixture of simple oxides as precursors in most of the mechanochemical reactions produced in a high-energy ball mill (in dry or wet mediums) an 80–95% of spinel phase can be produced, while the single ferritic phase can usually be obtained only with a posterior thermal annealing [5]. A drawback of the mechanochemical technique is that it is very difficult to obtain a localized size distribution [6] and that the particles exhibit a strong tendency for agglomeration [7]. In some cases, the wide size distribution and the agglomeration must be sorted out in order to make the particles useful for some particular applications, such as preparing ferrofluids. In this case, sonicating the resulting powder from the milling can

*Corresponding author. Tel.: +54 351 4334051 (103); fax: +54 351 4334054.
E-mail address: bercoff@famaf.unc.edu.ar (P.G. Bercoff).

http://dx.doi.org/10.1016/j.ceramint.2015.09.103
0272-8842/

break the agglomeration and centrifugating can allow the separation between microsized and nanosized particles.

On the other hand, while some chemical synthesis methods are appropriate for preparing nanoparticles with a sharp size distribution, most of them are very expensive and can provide only small amounts of powder. In this sense, milling is an economic alternative technique for the synthesis of nanoparticles on a larger scale.

Ferrofluids (FF) are stable colloidal dispersions of very fine magnetic particles with sizes in the lower nanometer range. The design and production of ferrofluids are currently under intensive investigation due to the broad applicability of such materials. Specifically designed FF are used in biomedical branches such as the cancer treatment by hyperthermia [8], MRI contrast agent [9], drug delivery [10], DNA hybridization [11] and cell separation [12]. One of the sound applications of biocompatible FF is magnetic hyperthermia. This effect relies on the ability of magnetic nanoparticles (NPs) to absorb power from a radio frequency (RF) field. This property is expressed by the specific absorption rate (SAR), which is the power absorbed per unit mass of magnetic NPs upon an ac field application. SAR depends on the amplitude and frequency of the RF field and on several properties of the NPs, such as saturation magnetization, magnetic volume, magnetic anisotropy and hydrodynamic volume; among others. The application of FF for hyperthermia treatment was investigated in the work of Chan et al. [13] and Jordan et al [14] in 1993. These studies experimentally prove the high efficiency of a superparamagnetic crystal suspension to absorb the energy of an alternating magnetic field and convert it into heat. Given that tumor cells are more sensitive to a temperature increase than healthy ones [14], this property can be used in vivo for increasing the temperature of tumor tissue and, in this way, destroy the pathological cells. Many efforts have been devoted in the last 20 years to improve hyperthermia for clinical applications. This technique is promising for cancer treatment because of the ease in targeting the cancerous tissue and hence having fewer side effects than chemotherapy and radiotherapy.

While the commonly used nanoparticles for hyperthermia are iron oxides such as maghemite and magnetite, in this work we propose the use of MnZn ferrites nanoparticles as an alternative, considering this compound has a high saturation magnetization, chemical stability and good biocompatibility.

This paper describes the evolution of the structure and magnetic properties during the mechanochemical processing of traditional precursors to form $Mn_{0.4}Zn_{0.6}Fe_2O_4$ nanoparticles. The smallest NPs were selected and modified in order to prepare a biocompatible and rather stable ferrofluid, suitable for hyperthermia treatments. It is shown that the mechanochemical method proves to be an interesting alternative to the wet-chemical processes for the synthesis of nanoparticles appropriate for this kind of applications.

2. Experimental

MnZn ferrite ($Mn_{0.4}Zn_{0.6}Fe_2O_4$) NPs were synthesized by the mechanochemical method in a *Fritsch Pulverisette 7* high-energy ball mill. The milling was performed at 600 rpm, with a ball/powder mass ratio of 20, in stainless steel vials with balls of the same material. The precursor powders of reagent grade – hematite (Fe_2O_3), zinc oxide (ZnO) and manganese oxide (MnO)– were milled from 15 to 120 min in stoichiometric proportions, according to the following reaction:

$$Fe_2O_3 + 0.6ZnO + 0.4MnO \rightarrow Zn_{0.6}Mn_{0.4}Fe_2O_4. \quad (1)$$

The samples resulting from the milling were named OX-*t*, being *t* the milling time in minutes ($t = 15$, 30, 45, 60, 90 and 120).

The samples' structural characterization was performed by X ray diffraction (XRD) with a Philips PW 3830 diffractometer, using Cu-Kα radiation. The magnetic properties were determined with a *Lake Shore 7300* vibrating sample magnetometer (VSM) at room temperature and with a maximum applied field of 1.5 kOe (1200 kA/m), and as a function of temperature with a *Cryogenics* cryostat. The size distribution and the morphology of samples were investigated with a field emission scanning electron microscope, FE-SEM SIGMA, Zeiss (LAMARX facilities). Transmission electron microscopy (TEM) was performed after dispersing the particles on carbon-coated copper grids using a high-resolution electron microscope EM 10 A/B (Zeiss) with operating voltage of 60 kV.

SAR (specific absorption rate) values were determined through time-dependent calorimetric measurements. SAR experiments were conducted in a clear Dewar glass containing 1 ml of FF located at the center of a 5 turns duty coil (25 mm inner diameter). The coil was fed with a 265 kHz ac current. In order to study the SAR dependence on field amplitudes (H_0), several measurements were performed at 150, 250, 400 and 500 Oe (12.2, 20.0, 31.7 and 39.4 kA/m). The temperature was determined with optic fiber sensors in contact with the FF and connected to a calibrated signal conditioner (*Neoptix*) with an accuracy of 0.1 K. The FF temperature was kept below 40 °C in order to minimize the fluid's evaporation and prevent its destabilization.

3. Results and discussion

3.1. Structural characterization

X ray diffractograms of the resulting powders from the milling are shown in Fig. 1. It is evident from the figure that the expected chemical reaction (Eq. (1)) starts before $t = 15$ min. The presence of hematite in the mixture decreases with milling time up to 120 min, when the remaining Fe_2O_3 is almost completely consumed by reaction (1).

The measured diffractograms prove that a Mn–Zn ferrite powder can be obtained directly from the milling without a thermal treatment in a very short time, since from 60 min of milling only 12% of hematite is present and wüstite has completely been removed from the powder. After 120 min of milling, only a small fraction ($< 5\%$) of hematite remains in the powder.

The samples' crystal sizes were calculated using Scherrer's formula:

$$D_{crystal} = \frac{0.88\lambda}{(\mathrm{FWHM} - F_M)\cos(\theta)}, \quad (2)$$

being $D_{crystal}$ the crystallite size, λ the diffractometer wavelength, FWHM the full width at half the maximum of the diffraction peak, F_M the experimental width in radians and θ the Bragg angle.

The calculated values of crystallite sizes using Eq. (2) for all samples take values around 12 nm (see Table 1 in Section 3.3). These values agree with results obtained in similar works in which the milling times are longer than 120 min [15]. Despite the milling, crystallite sizes remain almost unchanged from 15 to 120 min. At this point, it is worth mentioning that the values obtained with Scherrer's formula are estimative of the smallest crystallite sizes, which are usually smaller than particle sizes in polycrystalline powders.

3.2. Magnetic characterization

3.2.1. Magnetization vs. applied field

The specific magnetization (σ) as a function of the applied magnetic field (H) for samples OX-t was measured and is shown in Fig. 2 for all the samples.

A significant increase in σ is observed when increasing the milling time from 15 to 120 min. This effect is due to the increase of the ferrite percentage with milling time, in detriment of secondary phases.

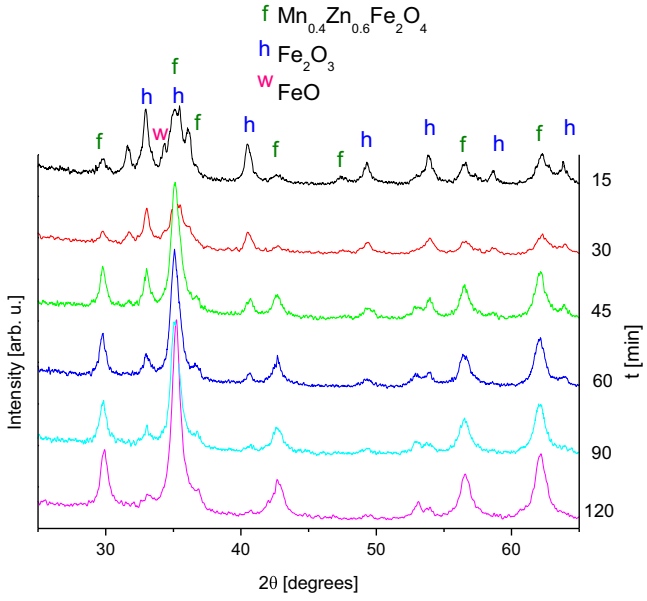

Fig. 1. Diffractograms of samples OX-t, with t = 15 to 120 min.

Table 1
Crystal sizes calculated from Scherrers's formula ($D_{crystal}$), and particle sizes and size distribution widths, from TEM measurements (D_{PT} and Δ_T), for different milling times, t.

t [min]	$D_{crystal}$ [nm]	D_{PT} [nm]	Δ_T [nm]
30	12 ± 2	–	–
45	12 ± 2	20 ± 1	10
60	12 ± 1	19 ± 1	11
90	11 ± 1	–	–
120	11 ± 1	15 ± 1	9

The inset in Fig. 2 shows that the specific saturation magnetization (σ_S) as a function of t ranges from 12.2 emu/g after 15 min to 50.3 emu/g after 120 min of milling. It is remarkable that after 60 min of milling, σ_S is about 70% of the highest attained value (50.3 emu/g) which is in good agreement with earlier works for similar NPs [16] and with bulk material [17]. During the milling process, the superficial chemical bonds are bound to be broken, but in this case, the very short time of synthesis prevents this effect, avoiding the diminishing magnetization saturation from bulk.

Coercive fields H_C and remanent magnetization M_R are nearly zero for all samples, in agreement with a superparamagnetic behavior. In order to have a deeper insight into the superparamagnetic effect, ZFC and FC curves were measured.

3.2.2. Magnetization vs. temperature

A superparamagnet has no remanence or coercivity and there is a temperature below which ferromagnetic order reappears, known as the blocking temperature (T_B). The maximum in the zero field cooling (ZFC) curve indicates the average blocking temperature, corresponding to the mean-sized particles. Below the blocking temperature, the effects of thermal energy decrease and ferromagnetic order is regained. The field cooling (FC) curve joins the ZFC curve in the superparamagnetic state at the irreversible temperature (T_{irr}). In most nanoparticulate magnetic systems, it is accepted that if T_{irr} is higher than T_B, the NPs are non-interacting [18].

ZFC–FC measurements of sample OX-120 were performed from 30 K to 280 K with an applied field of 200 Oe (16 kA/m). Specific magnetization σ as a function of temperature in the ZFC and the FC modes is shown in Fig. 3.

The average blocking and the irreversible temperatures were determined from Fig. 3, resulting T_B = 143 K and T_{irr} = 263 K. A wide T_B dispersion is observed, indicating a wide range of particle sizes. As the ZFC and FC curves separate at 263 K, the NPs are non-interacting above this temperature, which provides further evidence that the system is superparamagnetic at room temperature.

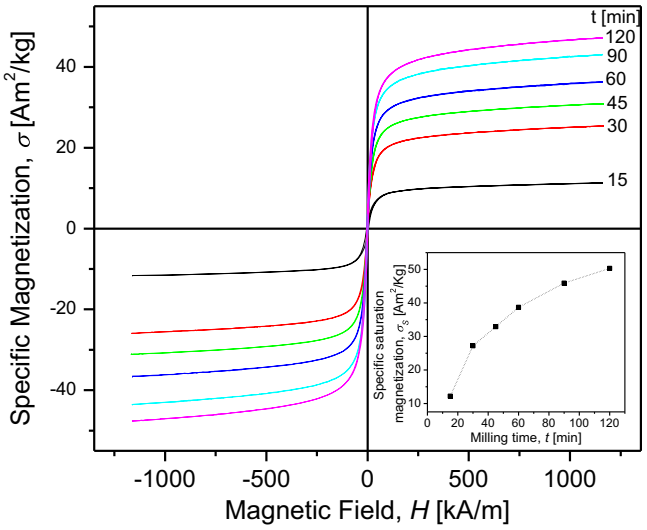

Fig. 2. σ vs. H curves for samples OX-t; for t = 15 to 120 min. The inset shows saturation magnetization values σ_S as a function of milling time, t.

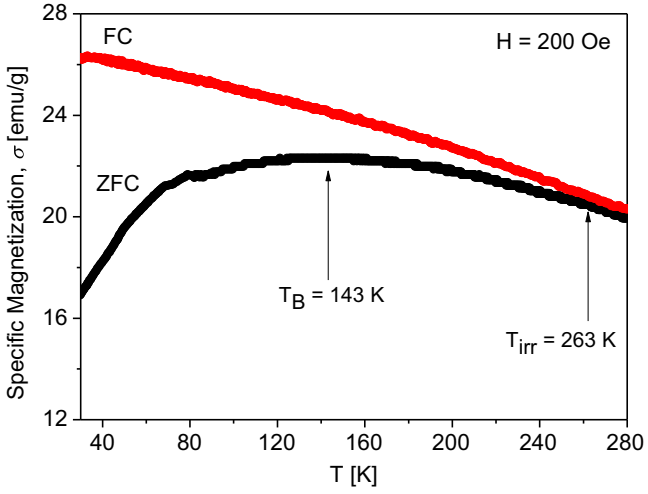

Fig. 3. σ vs. T curves for sample OX-120.

3.3. Particle size analysis

The analysis of the particle sizes and their distribution was performed using Scanning Electron Microscopy (SEM) and Transmission Electron Microscopy (TEM) data.

SEM images of samples OX-45, OX-90 and OX-120 are shown in Fig. 4(a)–(c) in the left panels. These images show that the powder resulting from the milling is composed of faceted particles which reduce their size as the milling time increases (as expected). The center panels of Fig. 4(a)–(c) shows TEM images of the same powders.

The particles diameters were measured from several TEM images. Over 200 particles were measured for each sample, with the aid of the *ImageJ* software [19]; the resulting histograms are shown in the right panels of Fig. 4(a)–(c). TEM images analyses indicate that the particle size distributions are log-normal with average particle diameters D_{PT} that vary from 20 nm for sample

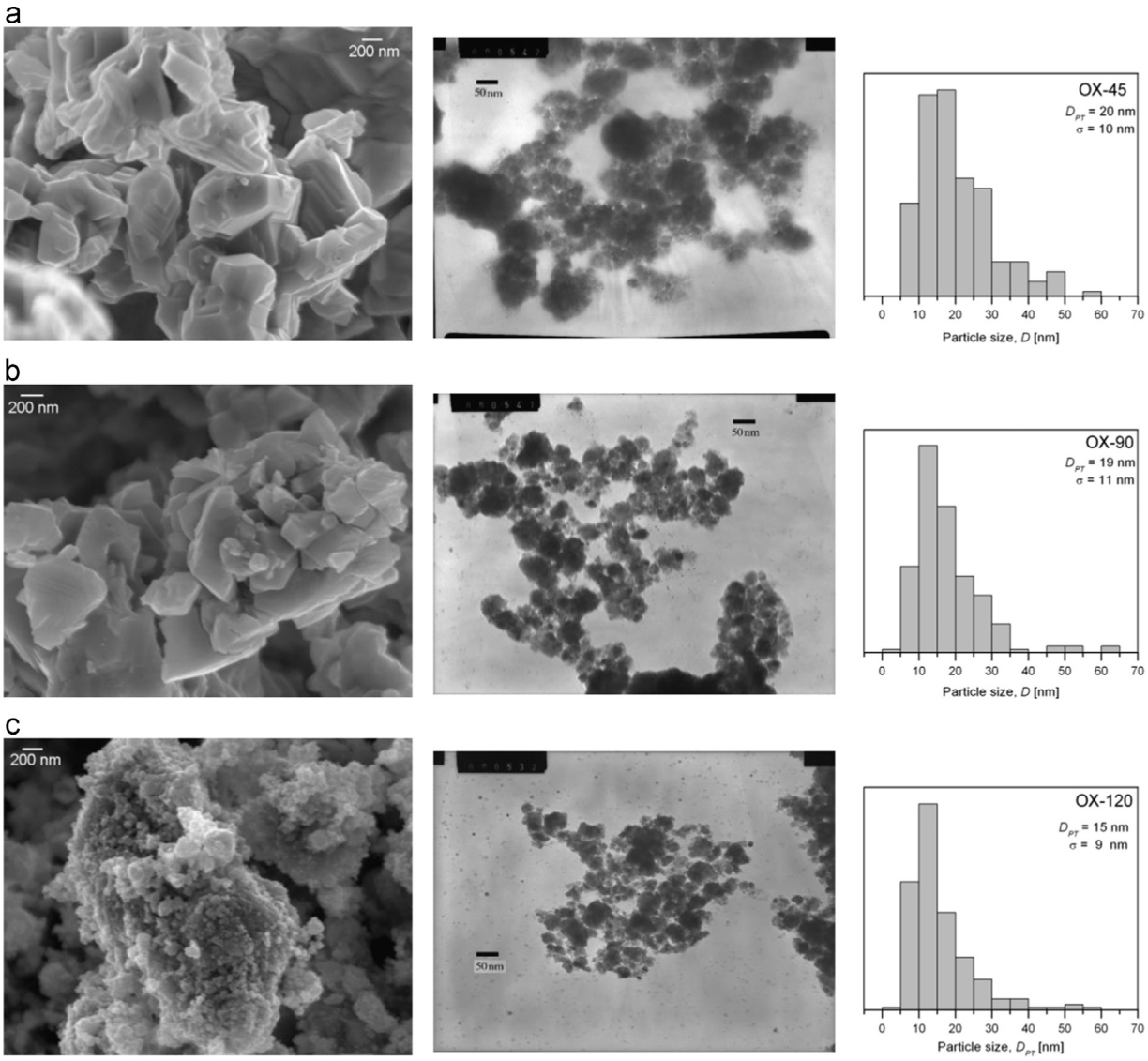

Fig. 4. Left panel: SEM images of the powders OX-t, for t=45 (a), 90 (b), and 120 min (c). Center panel: TEM images of OX-t, for t=45 (a), 90 (b), and 120 min (c). Right panel: histogram of the corresponding sample.

OX-45 to 15 nm for sample OX-120. Size values with the corresponding uncertainties and standard deviations, Δ_T, obtained from Fig. 4(a)–(c) are presented in Table 1.

The obtained particles sizes explain the superparamagnetic behavior observed in Figs. 2 and 3, as it has been reported previously [20] that the superparamagnetic limit for Mn–Zn ferrite particles is 20 nm.

Table 1 shows that no significant size decrease as a function of milling time in the crystallite sizes $D_{crystal}$ (calculated using the Scherrer formula) is observed, although this theoretical method is not sensitive to size distributions, and gives a size estimate of only the smallest particles in the powders. However, a decrease in mean particle size is observed from the values obtained from TEM measurements.

Despite the mean particle sizes of the powders are small enough for several applications (and in particular for hyperthermia) the rather large particle size distribution –inherent to the ball milling process– is undesirable for most of them. In order to solve this issue, the smallest particles were separated from the powders after the milling by centrifugation, using a mixture of hexane and ethanol with volume ratio of 1:2 as solvent [21].

The separated particles of sample OX-120 were chosen for the preparation of a ferrofluid.

3.4. Ferrofluid preparation

Surface activation of the nanoparticles for the coating procedure was first carried out in a basic media. The smallest particles of powder OX-120 were sonicated for 20 min in a 50% ammonia solution. After liquid decantation, the particles were suspended in a 2% chitosan solution in acetic acid sonicating for 6 hours in order to coat the particles surfaces with the biopolymer.

Fig. 5 shows a TEM image of coated Mn–Zn ferrite nanoparticles, named OX-120C, where the NPs are well coated and more disperse than before the coating (Fig. 4) and with a mean size of (8 ± 2) nm.

The coated particles were then re-suspended in a 0.5% chitosan solution. Stable solutions (for 12 h) were obtained with a concentration of 5.1 mg/ml. These results confirm that centrifugation of the powders is a good method for selecting the smallest particles and narrowing the dispersion.

In order to investigate the possibility of using this fluid for hyperthermia applications, Specific Absorption Rate (SAR) measurements were performed.

3.4.1. SAR results

The SAR of the nanoparticles in the fluid was retrieved from measurements of temperature T of the ferrofluid as function of time t, while an alternating magnetic field (AMF) was applied. SAR of the NPs in the fluid was calculated from the measured slopes, $\Delta T/\Delta t$, at 25 °C, using the expression [22]:

$$\mathrm{SAR} = \frac{C}{\phi}\Delta T/\Delta t, \quad \phi = \frac{m_{NP}}{m_{FF}}$$

where C is the FF specific heat, m_{FF} is the mass of the ferrofluid (1 mg) and m_{NP} is the mass of the magnetic NPs in the Dewar. For the studied ferrofluid, C was taken as that of water (4.1813 J/g K), being that a very good approximation owing to the low ϕ value (5.1×10^{-3}).

The SAR of the nanoparticles in the ferrofluid was measured for different AMF amplitudes ($H_0 = 12$, 20, 32 and 40 kA/m or 150, 250, 400 and 500 Oe) at the same frequency (265 kHz). The measured curves of T vs. t are shown in Fig. 6. The SAR values as function of the square of the AMF amplitude are shown in Fig. 7.

The highest SAR (of 80 W/g) was observed for the highest AMF amplitude. The obtained value is within the range of values observed in the literature for iron oxide nanoparticles [23,24].

Since SAR is strongly influenced by extrinsic parameters such as AMF amplitude and oscillatory frequency f, it is better to use the Intrinsic Loss Power (ILP) parameter [25] to compare the dissipation of different nanoparticle systems [26,27]. This parameter is defined as $\mathrm{ILP} = \mathrm{SAR}/H_0^2 f$ and it becomes quite independent of H_0 and f. However, it should be noted that this is not fully true [25,27]. This proclaimed independence is valid only in a region of low H_0, where the linear response theory is valid [22] and the SAR becomes proportional to the factor $H_0^2 f$. Above this limit, the slope of the

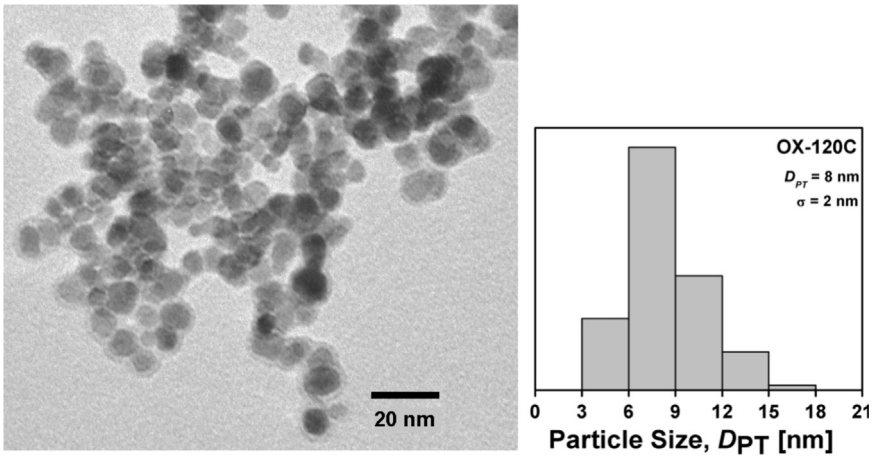

Fig. 5. TEM image of MnZn ferrite NPs with chitosan coating, OX-120C.

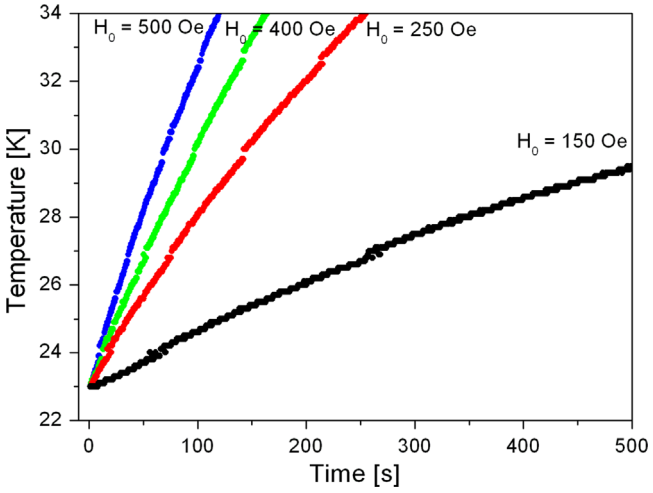

Fig. 6. Temperature increase due to the heating of 1 ml-OX-120C ferrofluid in a 265 kHz external alternating magnetic field, for several amplitudes: 12, 20, 32 and 40 kA/m (150, 250, 400 and 500 Oe).

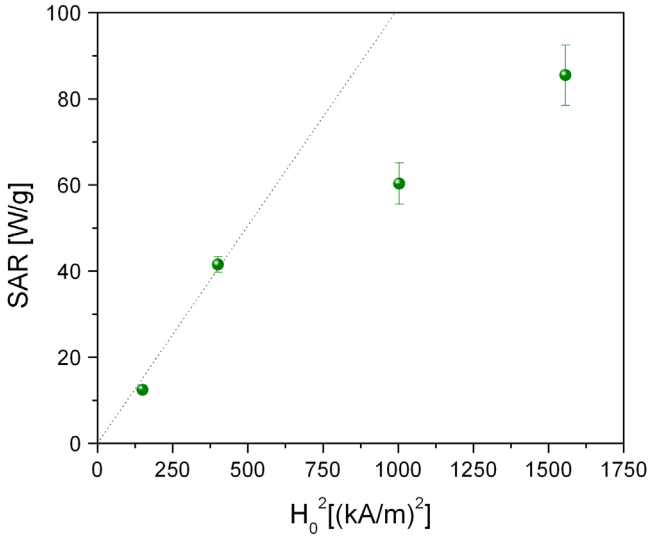

Fig. 7. SAR values as a function of H_0^2. The dotted line indicates the linear fit below 20 kA/m, obtained by means of a linear regression model without the intercept term.

SAR dependence on H_0^2 begins to diminish (see Fig. 7 above 500 $(kA/m)^2$) as consequence of the saturation behavior of the magnetic loop $M(H)$ [23,24]. Yet independence of frequency is still not ensured. Even for low AMF amplitudes, where a linear regime is valid, ILP depends on the out-of-phase magnetic susceptibility $\chi''(f)$ which, in fact, depends on the frequency. Arguing about this point and building on Rosensweig simulations [22], Kallumadil et al. –when proposing the ILP as a good comparison parameter [25]– assure that for polydisperse nanoparticles with polydispersity index greater than 0.1, the $\chi''(f)$ spectrum is broadened enough so as to make negligible the frequency dependence in a region of clinical interest (between 100 and 900 kHz).

Having these concepts in mind, the ILP for OX-120C was calculated from SAR vs. H_0^2 data (Fig. 7) in the linear response region (below 20 kA/m). In this region, the slope was

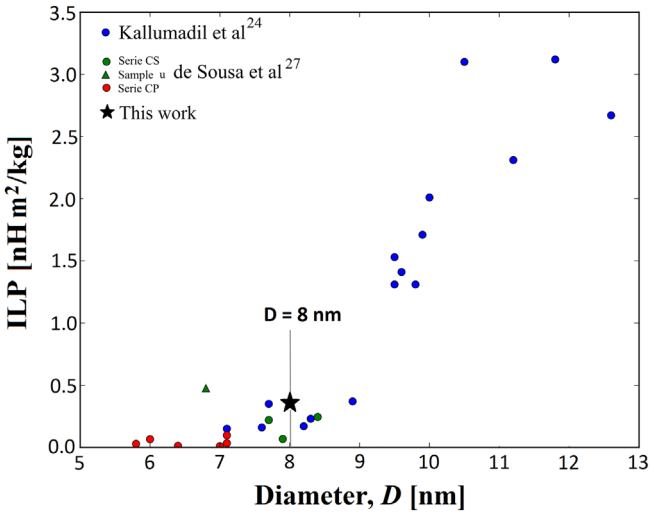

Fig. 8. ILP values for FFs with different sizes (Kallumadil et al. [25], de Sousa et al. [28] and this work).

determined using the least squares estimator of a linear regression model without the intercept term. The dashed line in Fig. 7 represents the fitting. The ILP, obtained by dividing the slope of the fitted line by the frequency of the magnetic field, gives (0.40 ± 0.03) nH m^2 kg^{-1}. Kallumadil et al. [25] made exhaustive ILP measurements for different commercially available iron oxide nanoparticles with different diameters and coatings, finding a good correlation between ILP and NPs diameter [25]. OX-120C ILP is in good agreement with small iron oxide nanoparticles with diameters between 7 and 9 nm [25] (see Fig. 8).

Both the OX-120C ILP and mean diameter (8 nm) determined in Section 3.4 are in very good agreement with the data from Kallumadil et al. This good agreement confirms a similar quality of this ferrofluid and nanoparticles as compared with well-established commercially available ones.

4. Conclusion

Mechanochemistry has proven to be effective for synthesizing ferrite nanoparticles in a short time. This low-cost technique can be easily implemented for obtaining large quantities of powder. Even when the repeated collisions with the balls produce structural damage on the nanoparticles, the same process leaves the particles' surface prone to be modified for coating and functionalization, making the NPs suitable for a ferrofluid preparation. A wide particle size distribution can be overcome by performing a selection amongst the particles, discarding the largest ones by centrifugation and keeping nanometric, rather monodisperse particles.

A biocompatible ferrofluid with the smallest NPs obtained from milling was successfully prepared. The magnetic nanofluid was stable for 12 h and shows a good performance for hyperthermia according to ILP results ((0.40 ± 0.03) nH m^2 kg^{-1}), making this fluid an excellent alternative to the usual and commercially available Fe-oxides ferrofluids used in this field.

Acknowledgments

The authors thank Secyt-UNC and CONICET for financing this work. M. Arana acknowledges a doctoral fellowship from CONICET.

References

[1] C. Suryanarayana, Mechanical alloying and milling, Prog. Mater. Sci. 46 (1–2) (2001) 1–184.
[2] L. Takacs, Self-sustaining reaction induced by ball milling, Prog. Mater. Sci. 47 (2002) 355–414.
[3] G.B. Schaffer, P.G. McCormick, Displacement reactions during mechanical alloying, Metall. Trans. A 21 (10) (1990) 2789–2794.
[4] J.S. Forrester, G.B. Schaffer, The chemical kinetics of mechanical alloying, Metall. Mater. Trans. A 26 (3) (1995) 725–730.
[5] I. Chicinas, Soft magnetic nanocrystalline powders produced by mechanical alloying routes, J. Optoelectron. Adv. Mater. 8 (2) (2006) 439–448.
[6] M. Khodaei, M.H. Enayati, F. Karimzadeh, Mechanochemically synthesized, 2002.
[7] M.J. Nasr Isfahani, M. Myndyk, D. Menzel, A. Feldhoff, J. Amighian, V. Šepelák, Magnetic properties of nanostructured MnZn ferrite, J. Magn. Magn. Mater. 321 (3) (2009) 152–156.
[8] M. Liangruksa, R. Ganguly, I.K. Puri, Parametric investigation of heating due to magnetic fluid hyperthermia in a tumor with blood perfusion, J. Magn. Magn. Mater. 323 (6) (2011) 708–716.
[9] H. Bin Na, I.C. Song, T. Hyeon, Inorganic nanoparticles for MRI contrast agents, Adv. Mater. 21 (21) (2009) 2133–2148.
[10] M. Mahmoudi, S. Sant, B. Wang, S. Laurent, T. Sen, Superparamagnetic iron oxide nanoparticles (SPIONs): development, surface modification and applications in chemotherapy, Adv. Drug Deliv. Rev. 63 (1–2) (2011) 24–46.
[11] J.-P. Lellouche, G. Senthil, A. Joseph, L. Buzhansky, I. Bruce, E.R. Bauminger, J. Schlesinger, Magnetically responsive carboxylated magnetite-polydipyrrole/polydicarbazole nanocomposites of core–shell morphology. Preparation, characterization, and use in DNA hybridization, J. Am. Chem. Soc. 127 (34) (2005) 11998–12006.
[12] I.K. Battisha, H.H. Afify, M. Ibrahim, Synthesis of Fe_2O_3 concentrations and sintering temperature on FTIR and magnetic susceptibility measured from 4 to 300 K of monolith silica gel prepared by sol–gel technique, J. Magn. Magn. Mater. 306 (2) (2006) 211–217.
[13] D.C.F. Chan, D.B. Kirpotin, P.A. Bunn, Synthesis and evaluation of colloidal magnetic iron oxides for the site-specific radiofrequency-induced hyperthermia of cancer, J. Magn. Magn. Mater. 122 (1–3) (1993) 374–378.
[14] A. Jordan, Inductive heating of ferromagnetic particles and magnetic fluids: physical evaluation for their potential for hyperthermia, Int. J. Hyperth. 25 (7) (2009) 512–516.
[15] L.J. Love, J.F. Jansen, T. McKnight, Y. Roh, T.J. Phelps, A magnetocaloric pump for microfluidic applications, IEEE Trans. Nanobiosci. 3 (2) (2004) 101–110.
[16] T. Verdier, V. Nivoix, M. Jean, B. Hannoyer, Characterization of nanocrystalline Mn–Zn ferrites obtained by mechanosynthesis, J. Mater. Sci. 39 (16/17) (2004) 5151–5154.
[17] H.P.J.W. Jan Smit, Ferrites: Physical Properties of Ferrimagnetic Oxides in Relation to their Technical Application, Wiley, New York, 1959.
[18] J.L. Dormann, D. Fiorani, E. Tronc, Magnetic relaxation in fine particle systems, in: I. Prigogine, S.A. Rice (Eds.), Advances in Chemical Physics, John Wiley and Sons, 1997, p. 345.
[19] W. Rasband, ImageJ, 2012. [Online]. Available: ⟨http://imagej.nih.gov/ij/index.html⟩ (accessed: 10-04-2015).
[20] K. Mandal, S. Chakraverty, S. Pan Mandal, P. Agudo, M. Pal, D. Chakravorty, Size-dependent magnetic properties of $Mn_{0.5}Zn_{0.5}Fe_2O_4$ nanoparticles in SiO_2 matrix, J. Appl. Phys. 92 (1) (2002) 501.
[21] B. Kowalczyk, I. Lagzi, B.A. Grzybowski, Nanoseparations: strategies for size and/or shape-selective purification of nanoparticles, Curr. Opin. Colloid Interface Sci. 16 (2) (2011) 135–148.
[22] R.E. Rosensweig, Heating magnetic fluid with alternating magnetic field, J. Magn. Magn. Mater. 252 (2002) 370–374.
[23] P.M. Zélis, G. a Pasquevich, S.J. Stewart, M.B.F. Van Raap, J. Aphesteguy, I.J. Bruvera, C. Laborde, B. Pianciola, S. Jacobo, F.H. Sánchez, Structural and magnetic study of zinc-doped magnetite nanoparticles and ferrofluids for hyperthermia applications, J. Phys. D: Appl. Phys. 46 (12) (2013) 125006.
[24] L.-M. Lacroix, R.B. Malaki, J. Carrey, S. Lachaize, M. Respaud, G. F. Goya, B. Chaudret, Magnetic hyperthermia in single-domain monodisperse FeCo nanoparticles: evidences for Stoner–Wohlfarth behavior and large losses, J. Appl. Phys. 105 (2) (2009) 023911.
[25] M. Kallumadil, M. Tada, T. Nakagawa, M. Abe, P. Southern, Q.A. Pankhurst, Suitability of commercial colloids for magnetic hyperthermia, J. Magn. Magn. Mater. 321 (10) (2009) 1509–1513.
[26] Q.A. Pankhurst, N.T.K. Thanh, S.K. Jones, J. Dobson, Progress in applications of magnetic nanoparticles in biomedicine, J. Phys. D. Appl. Phys 42 (22) (2009) 224001.
[27] R.R. Wildeboer, P. Southern, Q.A. Pankhurst, On the reliable measurement of specific absorption rates and intrinsic loss parameters in magnetic hyperthermia materials, J. Phys. D: Appl. Phys. 47 (49) (2014) 495003.
[28] M.E. de Sousa, M.B. Fernández van Raap, P.C. Rivas, P. Mendoza Zélis, P. Girardin, G.A. Pasquevich, J.L. Alessandrini, D. Muraca, F.H. Sánchez, Stability and relaxation mechanisms of citric acid coated magnetite nanoparticles for magnetic hyperthermia, J. Phys. Chem. C 117 (10) (2013) 5436–5445.